ARTICLE

SARS-CoV-2 Z-RNA activates the ZBP1-RIPK3 pathway to promote virus-induced inflammatory responses

Shufen Li[1,7], Yulan Zhang[1,7], Zhenqiong Guan[1,2,7], Meidi Ye[1,2], Huiling Li[1,2], Miaomiao You[1,2], Zhenxing Zhou[3], Chongtao Zhang[1], Fan Zhang[1], Ben Lu[4]✉, Peng Zhou[5]✉ and Ke Peng[1,2,6]✉

SARS-CoV-2 infection can trigger strong inflammatory responses and cause severe lung damage in COVID-19 patients with critical illness. However, the molecular mechanisms by which the infection induces excessive inflammatory responses are not fully understood. Here, we report that SARS-CoV-2 infection results in the formation of viral Z-RNA in the cytoplasm of infected cells and thereby activates the ZBP1-RIPK3 pathway. Pharmacological inhibition of RIPK3 by GSK872 or genetic deletion of MLKL reduced SARS-CoV-2-induced IL-1β release. ZBP1 or RIPK3 deficiency leads to reduced production of both inflammatory cytokines and chemokines during SARS-CoV-2 infection both in vitro and in vivo. Furthermore, deletion of ZBP1 or RIPK3 alleviated SARS-CoV-2 infection-induced immune cell infiltration and lung damage in infected mouse models. These results suggest that the ZBP1-RIPK3 pathway plays a critical role in SARS-CoV-2-induced inflammatory responses and lung damage. Our study provides novel insights into how SARS-CoV-2 infection triggers inflammatory responses and lung pathology, and implicates the therapeutic potential of targeting ZBP1-RIPK3 axis in treating COVID-19.

Cell Research (2023) 33:201–214; https://doi.org/10.1038/s41422-022-00775-y

INTRODUCTION

The severe acute respiratory syndrome coronavirus 2 (SARS-CoV-2), causative agent of the coronavirus disease 2019 (COVID-19),[1] has infected over 645 million people causing death of over 6.63 million worldwide by the time of December 13th, 2022. Most people infected by SARS-CoV-2 experienced mild symptoms including headache, loss of smell, dry cough, shortness of breath, fatigue, and fever.[2] However, approximately 5% of the COVID-19 patients develop critical conditions with severe lung damage.[3,4] Immunosuppression treatment for COVID-19 patients with hyperinflammation state has been proposed[5] and a number of clinical trials have been conducted to evaluate the efficacy of this strategy in COVID-19 therapy. However, ongoing progresses with general immunosuppressive drugs, such as dexamethasone, hydrocortisone, corticosteroids, have reported no or limited improvement in patients outcome.[6–10] Understanding the mechanisms of how SARS-CoV-2 triggers detrimental inflammatory responses is important for developing specific and effective therapeutic countermeasures against COVID-19.

Necroptosis is a lytic and proinflammatory form of cell death that can be triggered by various types of viruses.[11,12] Excessive necroptosis can lead to severe immune pathology.[13] A key mediator of necroptosis is receptor interacting protein (RIP) kinase (RIPK) 3 which contains a C-terminal RIP homotypic interaction motif (RHIM).[13] To initiate necroptosis, RIPK3 is first recruited through RHIM-dependent interactions by RIPK1, TIR-domain-containing adapter-inducing interferon (IFN) b (TRIF) or Z-nucleic acid (NA)-binding protein 1 (ZBP1),[14] leading to RIPK3-dependent phosphorylation of pseudokinase mixed lineage kinase domain-like protein (MLKL). Phosphorylated MLKL translocate into the plasma membrane and form channels through oligomerization, leading to lytic cell death. In addition to initiating necroptosis, RIPK3 has been reported to promote inflammatory signaling.[15] A recent study reports that RIPK3 mediates inflammatory signaling via its scaffolding instead of kinase activity. How RIPK3's kinase activity and scaffolding functionality regulate inflammatory responses in the context of virus infection remains to be investigated.

ZBP1, also known as DNA-dependent activator of interferon-regulatory factors (DAI), is an emerging innate sensor that senses infection of both DNA and RNA viruses and triggers multiple programmed cell death pathways including pyroptosis, apoptosis and necroptosis.[16] Studies with both RNA and DNA viruses reveal that the natural ligand of ZBP1 is the left-handed double-helical "Z-form" RNA (Z-RNA) structure.[14,17] Viral Z-RNAs form through different mechanisms. The binding of Vaccinia virus (VACV) E3 protein dsRBD domain with viral dsRNA genome promotes the formation or stabilization of Z-RNA.[14,18] Alternatively, virus Z-RNA can form when viral dsRNA adopts the z-conformation as in the case of influenza A virus (IAV) defective viral genomes.[17] It has been reported that SARS-CoV-2 replication leads to dsRNA formation,[19] but whether the viral dsRNA can adopt the conformation of Z-RNA and/or plays a role in triggering viral pathogenesis is currently unknown.

[1]State Key Laboratory of Virology, Center for Antiviral Research, Wuhan Institute of Virology, Chinese Academy of Sciences, Wuhan, Hubei, China. [2]University of Chinese Academy of Sciences, Beijing, China. [3]University of Science and Technology of China, Hefei, Anhui, China. [4]Department of Hematology and Critical Care Medicine, The 3rd Xiangya Hospital, Central South University, Changsha, Hunan, China. [5]Guangzhou Laboratory, Guangzhou, Guangdong, China. [6]Hubei Jiangxia Laboratory, Wuhan, Hubei, China. [7]These authors contributed equally: Shufen Li, Yulan Zhang, Zhenqiong Guan. ✉email: xybenlu@csu.edu.cn; zhou_peng@gzlab.ac.cn; pengke@wh.iov.cn

Received: 20 June 2022 Accepted: 28 December 2022
Published online: 17 January 2023

Here, we report that SARS-CoV-2 infection results in production of Z-RNA which binds and activates the ZBP1-RIPK3 pathway. Pharmacological inhibition of RIPK3 by GSK872 or genetic deletion of MLKL significantly reduced interleukin-1 beta (IL-1β) release but did not affect chemokine production. In contrast, depletion of ZBP1 or RIPK3 strongly reduced both inflammatory cytokine secretion and chemokine production. Using adenovirus human Angiotensin Converting Enzyme-2 (hACE2)-transduced mouse model, we report here that SARS-CoV-2-infected Zbp1$^{-/-}$ or Ripk3$^{-/-}$ mice displayed markedly attenuated inflammatory cytokine and chemokine production, reduced immune cell infiltration and alleviated lung damage as compared to that of infected Mlkl$^{-/-}$ or control mice. Thus, the ZBP1-RIPK3 axis plays a critical role in SARS-CoV-2-induced inflammatory responses. These results also indicate the ZBP1-RIPK3 pathway as a novel target for anti-inflammation therapy for COVID-19.

RESULTS

SARS-CoV-2 infection upregulates the expression of ZBP1 to stimulate inflammatory signaling and necroptosis

To investigate the mechanisms of SARS-CoV-2-triggered inflammatory response, we first determined the virus growth curve on the Calu-3 cells, an established lung epithelial cell model for studying SARS-CoV-2 replication and pathogenesis.[19–21] It is found that SARS-CoV-2 productively infected Calu-3 cells and virus production increased overtime (Fig. 1a). The transcriptomic analysis of SARS-CoV-2-infected Calu-3 cells revealed NF-κB activation and upregulation of a panel of proinflammatory cytokines (Fig. 1b), further supporting Calu-3 being a suitable cell model for studying inflammatory responses induced by SARS-CoV-2 infection. Annexin V/propidium iodide (PI) staining revealed that virus infection induced pronounced cell death (Supplementary information, Fig. S1a). Necroptosis is a form of inflammatory cell death mediated by MLKL, the activation of which was monitored by analyzing the phosphorylation of MLKL (pMLKL).[22,23] pMLKL was observed in SARS-CoV-2-infected cells (Supplementary information, Fig. S1b) and immunofluorescence assay (IFA) with antibody detecting phosphorylated MLKL revealed distinct localization of pMLKL on the plasma membrane, consistent with its translocation upon necroptosis activation (Supplementary information, Fig. S1c).

RNA-seq analysis revealed the upregulation of ZBP1 during SARS-CoV-2 infection (Fig. 1c), which was confirmed by quantitative reverse transcriptase PCR (qRT-PCR) and western blot analysis (Fig. 1d, e). ZBP1 has been reported as a cytoplasmic Z-nucleic acid sensor with the capacity to activate NF-κB signaling pathway and to induce necroptosis through promoting RIPK3 activation.[24,25] To investigate whether ZBP1 contributes to SARS-CoV-2-induced inflammatory signaling and necroptosis, ZBP1 was depleted through CRISPR-Cas9-mediated knockout (KO) in Calu-3 cells followed by SARS-CoV-2 infection. Depletion of ZBP1 did not affect SARS-CoV-2 viral load (Supplementary information, Fig. S2a) but reduced virus-induced MLKL phosphorylation indicating its role in the activation of necroptosis (Fig. 1f). PI and Annexin V staining showed that depletion of ZBP1 reduced SARS-CoV-2-triggered cell death (Supplementary information, Fig. S2b). Depletion of ZBP1 also significantly reduced release of the matured form of IL-1β (P17) (Fig. 1f), supporting that the necroptosis pathway contributes to inflammatory cytokine release during SARS-CoV-2 infection. Western blot analysis showed that depletion of ZBP1 reduced the cleavage of PARP1 and Caspase3 (Fig. 1f). Furthermore, the transcriptional level of a series of proinflammatory cytokines and chemokines, including IL-1β, CCL2 and CXCL2, etc., were also reduced in SARS-CoV-2-infected ZBP1 KO cells (Fig. 1g). These results suggest that ZBP1 contributes to SARS-CoV-2-triggered inflammatory signaling and necroptosis activation.

SARS-CoV-2 infection generates Z-RNA to activate ZBP1

ZBP1 is a nucleic acid sensor that triggers inflammatory responses through binding Z-DNA or Z-RNA (Z-NA) via Zα domains.[14,17] We therefore asked whether Z-NA was generated during SARS-CoV-2 infection to activate ZBP1. Recently, a study identified antibodies that can recognize Z-RNA and reported Z-RNA generated by influenza virus as the natural ligand for ZBP1.[17] We used the same antibody to analyze whether SARS-CoV-2 infection can trigger Z-NA formation. Labeling SARS-CoV-2-infected cells with Z-NA antibody revealed generation of Z-NA signals in the cytoplasm (Fig. 2a), indicative of the formation of Z-NA during virus infection. Treatment with RNase A strongly reduced the Z-NA signal (Fig. 2b, d) while DNase I treatment showed no significant effect on the accumulation of Z-NA signal (Fig. 2c, d), suggesting that the detected cytoplasmic Z-NA within SARS-CoV-2-infected cells was Z-RNA. The formation of Z-RNA during the infection of other variants of concern (VOCs), including SARS-CoV-2 Alpha, Beta, Delta and Omicron strains was also observed (Fig. 2e). Furthermore, a distinct co-localization between ZBP1and Z-RNA was observed in infected cells (Fig. 2f, g). Next, we used the Z-NA antibody to capture Z-RNAs formed in SARS-CoV-2-infected Calu-3 cells. Cell lysate from SARS-CoV-2-infected Calu-3 cells was incubated with Z-NA antibody followed by immunoprecipitation, DNase I treatment and qRT-PCR analysis. The results showed that the region of SARS-CoV-2 genome ORF1a and ORF1b is enriched by the Z-NA antibody, indicating formation of Z-RNA in this region of viral RNA (Fig. 2h). These results together suggest that the SARS-CoV-2-induced Z-RNA might serve as a ligand to activate ZBP1 during infection.

ZBP1 promotes SARS-CoV-2 pathogenesis in vivo

Next, we analyzed whether ZBP1 mediates SARS-CoV-2 pathogenesis in infected mouse model. Zbp1$^{-/-}$ or control mice were first transduced with adenovirus vectors encoding human ACE2 (Ad5-hACE2) to allow productive SARS-CoV-2 infection, an established mouse model for studying SARS-CoV-2 replication and infection-related pathology.[26] At 2 days post infection (dpi), lung samples were collected and subjected to quantitative PCR analysis. ACE2 expression level was comparable among the experimental groups (Supplementary information, Fig. S3). ZBP1 depletion did not affect SARS-CoV-2 replication, but the expression of proinflammatory cytokines and chemokines, including IL-6, CXCL10, CCL2, CCL4, etc., was significantly reduced compared with the control (Fig. 3a). Hematoxylin-eosin (H&E) staining of lung sections revealed inflammatory cell infiltration and expanded alveolar septa in SARS-CoV-2-infected control mice (Fig. 3b). ZBP1 depletion alleviated SARS-CoV-2-induced immune cell infiltration and alveolar septa expansion (Fig. 3b). Infiltration of leukocyte in the lung of Zbp1$^{-/-}$ mice was strongly reduced compared with infected control mice (Fig. 3c, d), as indicated by the staining of CD45 with immunohistochemistry analysis. Staining of CD68 (Fig. 3e, f), MPO (Fig. 3g, h) and CD3 (Fig. 3i, j) revealed decreased recruitment of macrophages, neutrophils and T cells in the lung of Zbp1$^{-/-}$ mice infected by SARS-CoV-2, respectively. Immunohistochemistry assay analyzing CD4- and CD8-positive cells was performed to identify the T cell types that infiltrate into the SARS-CoV-2-infected lung tissues. The results showed that ZBP1 depletion reduced infiltration of both T cell types in the lung tissue and the CD8^{+} T cell infiltration was reduced more pronouncedly (Supplementary information, Fig. S4). Taken together, these results suggested that ZBP1 promotes SARS-CoV-2-induced pathogenesis in infected mouse model.

Inflammatory signaling is regulated by the ZBP1-RIPK3 axis

Next, we investigated the mechanism by which ZBP1 promotes inflammatory signaling and necroptosis activation during SARS-CoV-2 infection. RIPK3 has been reported to be involved in ZBP1-induced NF-κB signaling pathway and necroptosis.[27,28] Staining of lung sections of SARS-CoV-2-infected mice showed that depletion

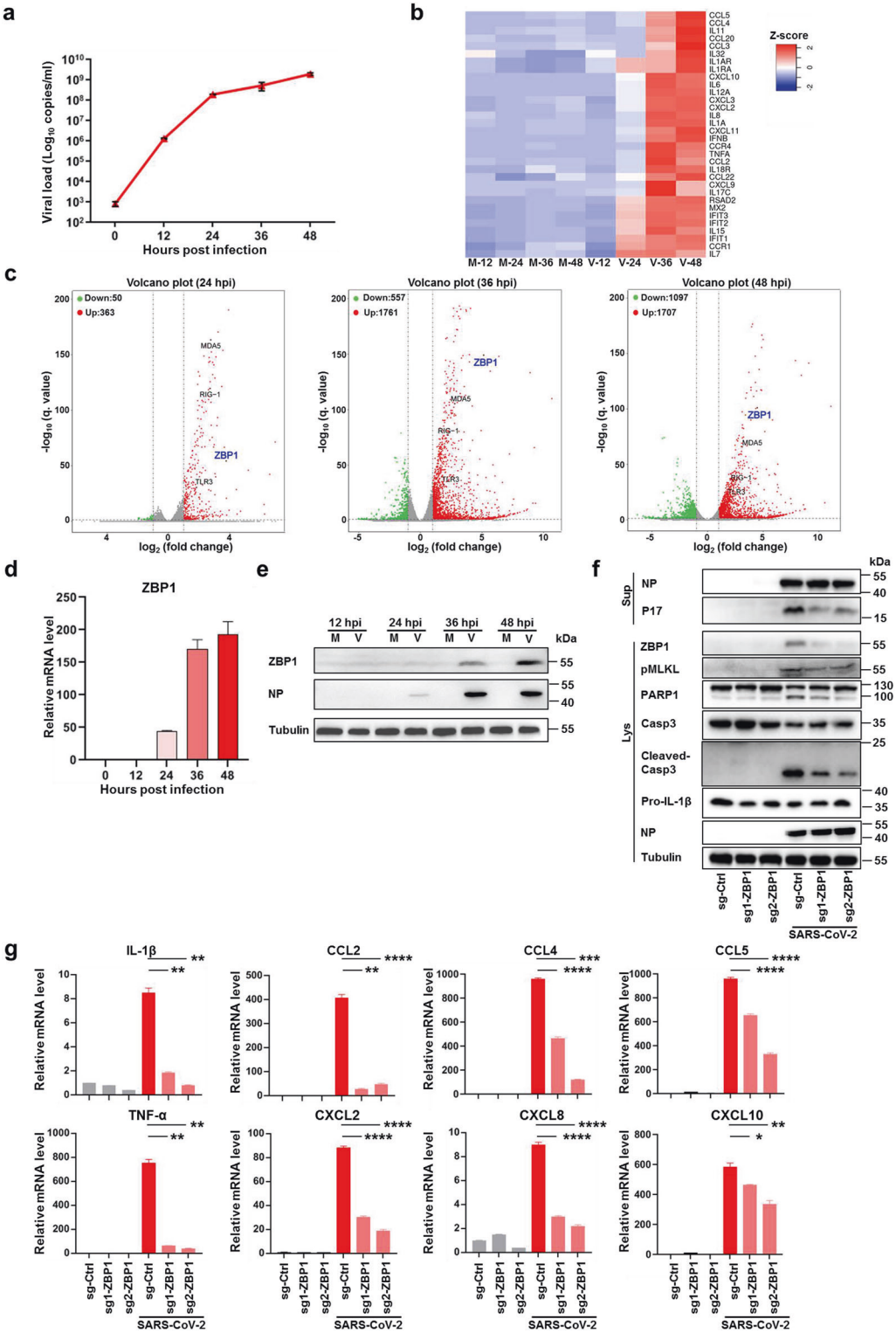

Fig. 1 SARS-CoV-2 infection upregulates ZBP1 to stimulate inflammatory signaling and necroptosis. a–**e** Calu-3 cells were infected with SARS-CoV-2 (MOI = 0.1) or mock treated, cells and supernatants were harvested at the indicated times. Extracellular vRNA levels were determined with quantitative RT-PCR (qRT-PCR) (**a**). **b**, **c** Transcriptomic analysis of infected cells harvested at the indicated times. Heat map profiling expression of inflammation regulated genes that were significantly upregulated upon SARS-CoV-2 infection (**b**). M, mock, V, virus infection. Volcano plot indicating differentially expressed genes. Red and green indicated up- and downregulated genes, respectively (**c**). The transcription (**d**) and expression (**e**) level of ZBP1 was determined by qRT-PCR and western blot assay. **f**, **g** Calu-3 cells stably expressing non-targeting sgRNA (scramble) or sgRNAs against ZBP1 were infected with SARS-CoV-2 (MOI = 0.1). Cells and supernatants were harvested at 48 hpi. NP and P17 levels in supernatants and expression levels of ZBP1, pMLKL, PARP1, Casp3, cleaved-Casp3, pro-IL-1β or NP in cell lysates were measured by western blot assay (**f**). Total RNA was extracted and relative mRNA level of indicated cytokine and chemokine genes were detected by qRT-PCR (**g**). Data shown are means ± SEM. Statistical significance was analyzed by Student's *t*-test. $^{*}P < 0.05$; $^{**}P < 0.01$; $^{***}P < 0.001$; $^{****}P < 0.0001$.

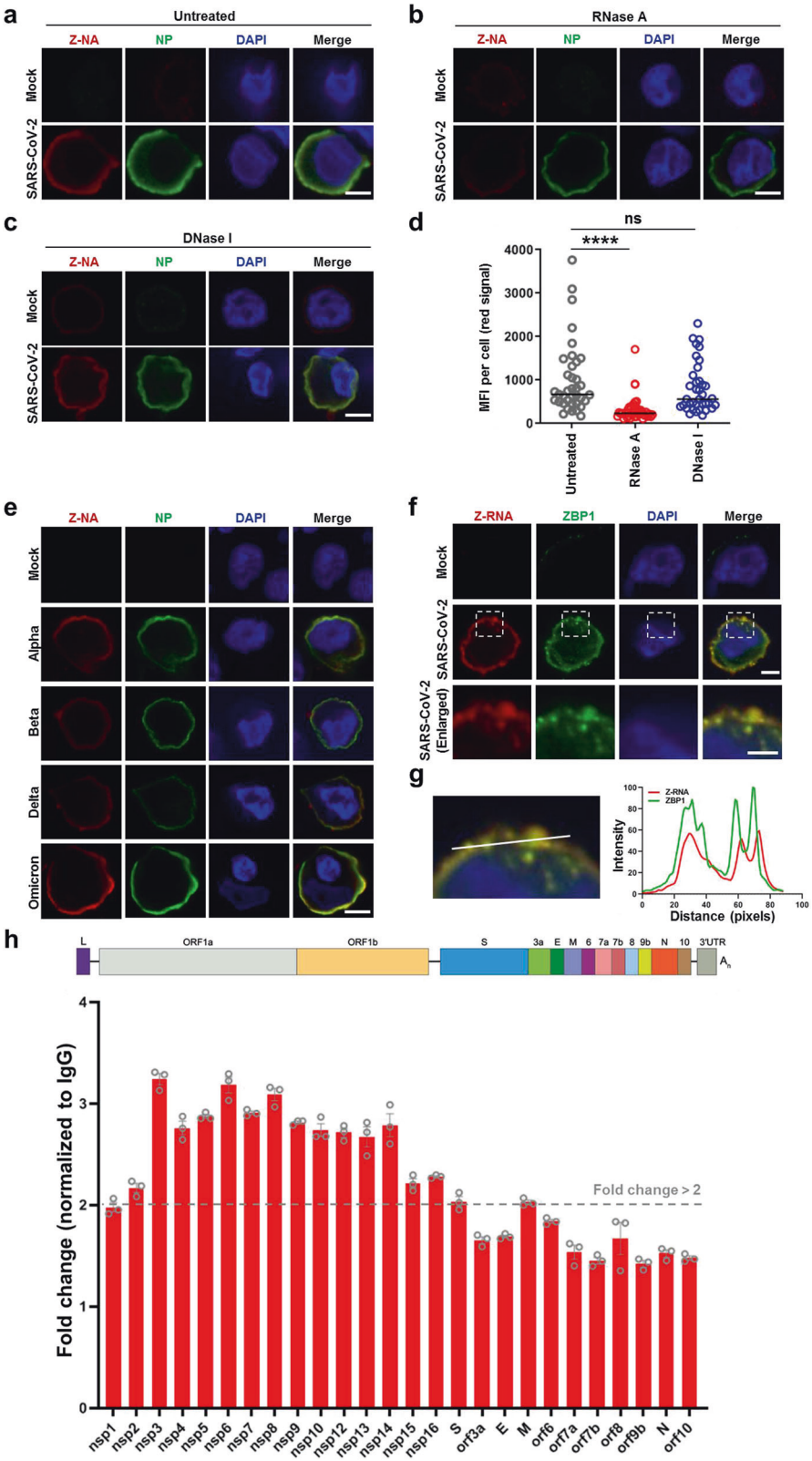

of ZBP1 reduced RIPK3 phosphorylation (Supplementary information, Fig. S5). Therefore we analyzed its potential role in SARS-CoV-2-induced inflammatory signaling and necroptosis. RIPK3 was depleted in Calu-3 cells through stable expression of shRNA and western blot analysis confirmed the depletion of RIPK3 (Fig. 4a). PI and Annexin V staining showed that knockdown of RIPK3 reduced SARS-CoV-2-triggered cell death (Supplementary information, Fig. S6a). Western blot analysis showed that knockdown of RIPK3 also reduced the cleavage of PARP1 and Caspase3 (Fig. 4a). The SARS-CoV-2 viral loads were comparable between RIPK3

Fig. 2 Formation of Z-RNA during SARS-CoV-2 infection. a–d SARS-CoV-2 original strain (MOI = 0.1) infected or uninfected (mock) Calu-3 cells were fixed and permeabilized at 48 hpi, and then either untreated (**a**) or treated with RNase A (**b**) or DNase I (**c**). Cells were co-stained with antibodies against Z-NA (red) and viral antigen NP (green). Nuclei were stained by DAPI (blue). **d** Quantification of the median florescence intensity (MFI) of Z-NA staining in SARS-CoV-2-infected cells in **a**–**c**. Comparison of median values between two groups was analyzed by Mann–Whitney test. ****$P < 0.0001$; ns, no significance. Scale bar, 10 μm. **e** Calu-3 cells were infected with SARS-CoV-2 Alpha, Beta, Delta and Omicron strains (MOI = 0.1) for 48 h, and stained with antibodies against Z-NA (red) and NP (green). Scale bar, 10 μm. **f** SARS-CoV-2 original strain infected Calu-3 cells were co-stained with Z-NA and ZBP1 antibodies. Scale bars, 10 μm and 5 μm in enlarged image. **g** Quantitative analysis of the co-localization between Z-RNA and ZBP1 was performed with ImageJ. **h** Identification of viral derived Z-RNA. Calu-3 cells infected with SARS-CoV-2 (MOI = 0.1) for 48 h were lysed and incubated with Z-RNA antibody or isotype mouse IgG for immunoprecipitation. Enriched RNA was subjected to qRT-PCR analysis.

knockdown and control cells (Supplementary information, Fig. S6b) but virus-induced expression of IL-1β, tumor necrosis factor alpha (TNF-α), IL-6, CCL2 and CXCL8 was significantly reduced in RIPK3 knockdown cells as compared to that of the control cells (Fig. 4b). Silencing of RIPK3 expression also significantly inhibited MLKL phosphorylation concomitantly with reduced IL-1β P17 secretion (Fig. 4a), indicating that RIPK3 is important for SARS-CoV-2-induced MLKL phosphorylation and necroptosis activation. To further explore the role of necroptosis in SARS-CoV-2-induced inflammation, MLKL was depleted in Calu-3 cells using CRSPR-Cas9. In line with activation of MLKL-mediated necroptosis, PI and Annexin V staining showed that depletion of MLKL reduced SARS-CoV-2-triggered cell death (Supplementary information, Fig. S6c). Western blot analysis showed that depletion of MLKL also reduced the cleavage of PARP1 and Caspase3 (Fig. 4c), indicating the possibility of promotion of apoptosis by necroptosis during SARS-CoV-2 infection. MLKL depletion did not affect SARS-CoV-2 viral load (Supplementary information, Fig. S6d) but reduced SARS-CoV-2-induced IL-1β P17 release (Fig. 4c). However, in contrast to RIPK3 depletion, the inflammatory cytokine and chemokine production was not affected by MLKL deficiency (Fig. 4d). Furthermore, treatment of SARS-CoV-2-infected cells with GSK872, an inhibitor of RIPK3 kinase activity, significantly inhibited MLKL phosphorylation and IL-1β P17 release (Fig. 4e), but showed no inhibition on the production of proinflammatory cytokines and chemokines (Fig. 4f). Together, these results indicated that while the kinase activity of RIPK3 determines necroptosis activation, its scaffolding functionality mediated the inflammatory signaling during SARS-CoV-2 infection.

To investigate the regulatory mechanism of ZBP1-RIPK3-triggered inflammatory responses, we reconstituted ZBP1 KO Calu-3 cells with FLAG-tagged full-length ZBP1 (ZBP1), or ZBP1 truncation mutants deleted of Zα2 domain or RHIM domain (ZBP1-ΔZα2 or ZBP1-ΔRHIM, respectively). The Zα2 and RHIM domains are known to mediate ZBP1 binding with Z-RNA or with RIPK3, respectively.[17] We performed SARS-CoV-2 infection of these cells and precipitated ZBP1 in pulldown experiment with the FLAG tag. The results showed that in cells expressing full-length ZBP1, ZBP1-FLAG precipitated with RIPK3 and MLKL (Fig. 4g). MLKL phosphorylation and IL-1β release were also observed in SARS-CoV-2-infected Calu-3 cells reconstituted with full-length ZBP1 (Fig. 4h). In contrast, in ZBP1 KO Calu-3 cells reconstituted with ZBP1-ΔZα2 or ZBP1-ΔRHIM, truncated ZBP1 did not precipitate with RIPK3 or MLKL (Fig. 4g). MLKL phosphorylation and IL-1ß release were also not observed in these cells (Fig. 4h). These results suggested that both Zα2 and RHIM domains are important for ZBP1-RIPK3-mediated inflammatory responses triggered by SARS-CoV-2 infection.

The scaffolding functionality of RIPK3 promotes chemokine production during SARS-CoV-2 infection in vivo

Next, we investigated whether RIPK3 regulates inflammatory responses during SARS-CoV-2 infection in vivo. For this purpose, control, Ripk3$^{-/-}$ and Mlkl$^{-/-}$ mice were transduced with the Ad5-hACE2 to allow productive SARS-CoV-2 infection. At 2 dpi, lung samples were collected and cytokines and chemokines were analyzed with qRT-PCR assay. Similar to ZBP1 depletion, SARS-CoV-2 replication was comparable between control and Ripk3$^{-/-}$ mice, but the expression of proinflammatory cytokines and chemokines, including IL-6, CXCL10, CCL2, CCL4, etc., was significantly reduced in the infected Ripk3$^{-/-}$ mice (Fig. 5a). In contrast, MLKL deficiency exhibited no inhibition on the upregulation of the indicated cytokines and chemokines triggered by SARS-CoV-2 infection (Fig. 5a). These results indicate that RIPK3 is important for SARS-CoV-2-triggered inflammation in vivo and are in line with the in vitro observations that the scaffolding functionality of RIPK3 is critical for SARS-CoV-2-induced inflammatory signaling.

To further analyze whether the kinase activity of RIPK3 is dispensable for SARS-CoV-2-induced inflammatory signaling, BALB/c mice was infected with a mouse-adapted SARS-CoV-2 virus strain (WBP-1)[29] with GSK872 treatment. Briefly, BALB/c mice were intranasally inoculated with WBP-1, and GSK872 was given by intraperitoneal injection after inoculation on a daily basis. Lung tissue homogenates harvested at 5 dpi were analyzed. GSK872 treatment strongly reduced MLKL phosphorylation in the lung of infected mice confirming the efficacy of drug treatment (Supplementary information, Fig. S7a). In contrast, GSK872 treatment did not affect viral replication or the expression of proinflammatory cytokines and chemokines (Fig. 5b). Similar results were observed in the Ad5-hACE2 -transduced mouse model infected by SARS-CoV-2 with or without GSK872 treatment (Supplementary information, Fig. S7b, c). These results together suggested that the scaffolding functionality instead of the kinase activity of RIPK3 is critical for proinflammatory cytokine and chemokine production during SARS-CoV-2 infection in vivo.

RIPK3 contributes to immune cell infiltration and lung damage during SARS-CoV-2 infection

Since RIPK3 deficiency results in reduced inflammatory signaling in SARS-CoV-2-infected mouse model, we investigated whether RIPK3 also mediates SARS-CoV-2 pathogenesis in vivo. Ripk3$^{-/-}$, Mlkl$^{-/-}$ and control mice were transduced with Ad5-hACE2 and then infected with SARS-CoV-2. Staining of lung sections of SARS-CoV-2-infected mice showed that depletion of ZBP1 and RIPK3, but not MLKL, reduced RIPK3 phosphorylation, while depletion of ZBP1, RIPK3, and MLKL all reduced MLKL phosphorylation and caspase3 cleavage (Supplementary information, Figs. S5 and S8). H&E staining of lung sections revealed pronounced inflammatory cell infiltration and expanded alveolar septa in SARS-CoV-2-infected control mice (Fig. 6a). RIPK3 depletion, but not MLKL depletion, strongly reduced SARS-CoV-2-induced immune cell infiltration and alveolar septa expansion (Fig. 6a). Compared with wild-type control, infiltration of leukocyte in the lung of infected mice was reduced in both Ripk3$^{-/-}$ and Mlkl$^{-/-}$ mice, while RIPK3 depletion resulted in a more pronounced reduction (Fig. 6b, c). Staining of CD68 (Fig. 6d, e), and CD3 (Fig. 6f, g) revealed decreased recruitment of macrophages and T cells in the lung of infected Ripk3$^{-/-}$ mice, while recruitment was similar between infected control and Mlkl$^{-/-}$ mice (Fig. 6d, f). SARS-CoV-2 infection-induced neutrophil infiltration was reduced in Zbp1$^{-/-}$, Ripk3$^{-/-}$, and Mlkl$^{-/-}$ mice compared with infected control mice,

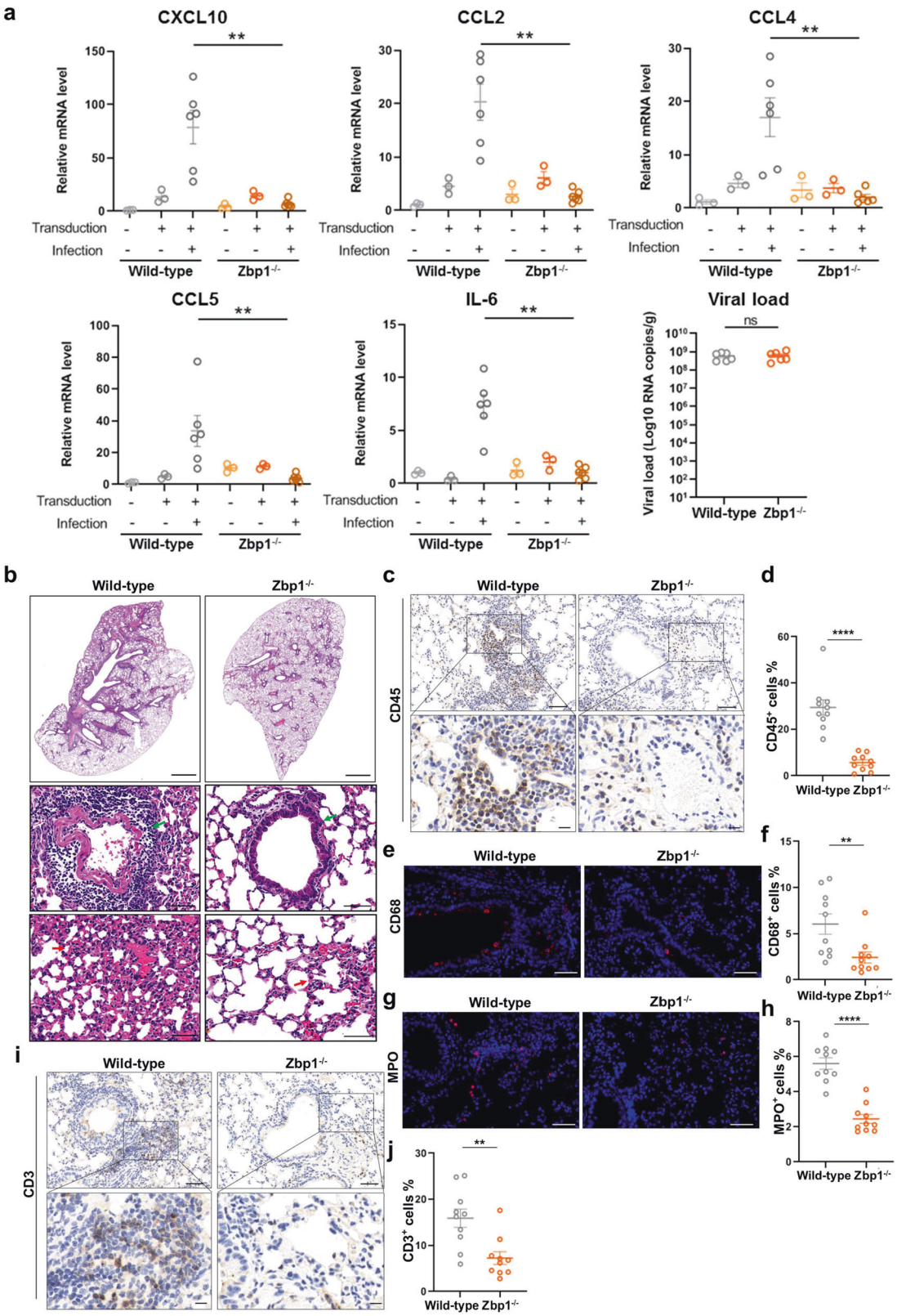

of which reduction is more pronounced in Zbp1$^{-/-}$ and Ripk3$^{-/-}$ mice (Figs. 3g, h and 6h, i).

Similar to SARS-CoV-2-infected Zbp1$^{-/-}$ mice, RIPK3 depletion reduced infiltration of both CD4^{+} and CD8^{+} T cell types in the lung tissue (Supplementary information, Fig. S9). A recent study of SARS-CoV-2 pathogenesis in rhesus macaque model proposed that virus-induced CD8^{+}CXCR3^{+} cell infiltration into the lung is important for virus-triggered lung damage.[30] Since RIPK3

Fig. 3 ZBP1 promotes SARS-CoV-2-induced inflammatory signaling and lung damage. a–j $Zbp1^{-/-}$ and wild-type mice were divided into three groups: Ad5-hACE2 non-transduced and non-infected ($n = 3$), transduced but non-infected ($n = 3$), transduced and infected ($n = 6$). Mice were intranasally transduced with Ad5-hACE2 (2.5×10^8 PFU) and infected with SARS-CoV-2 (1×10^5 $TCID_{50}$) at 5 days post transduction. Lung samples were harvested at 2 dpi. **a** Relative level of indicated genes was analyzed with qRT-PCR and normalized to non-transduced and uninfected wild-type controls. Data shown are means ± SEM. Statistical significance was analyzed by Student's *t*-test. $^{**}P < 0.01$; ns, no significance. **b** The histopathological changes in lung were evaluated by H&E staining. Scale bars, 1000 μm and 50 μm in enlarged image. Inflammatory cell infiltration (green arrow) and alveolar septa expansion (red arrow) were observed in the lung sections. Immunostaining of CD45 (**c**), CD68 (**e**), MPO (**g**) and CD3 (**i**) representing the infiltration of leukocytes, macrophages, neutrophils and T cells, respectively. **c**, **i** Scale bars, 50 μm and 10 μm in the enlarged image. **e**, **g** Scale bars, 50 μm. **d**, **f**, **h**, **j** Quantitative analysis of positive cells was performed with ImageJ for **c**, **e**, **g**, **i**, respectively. Data shown are means ± SEM. Statistical significance was analyzed by Student's *t*-test. $^{**}P < 0.01$; $^{****}P < 0.0001$.

depletion leads to reduced CXCL10 upregulation, the ligand of CXCR3, during SARS-CoV-2 infection, we analyzed the presence of $CD8^+CXCR3^+$ cells in SARS-CoV-2-infected control and $Ripk3^{-/-}$ mice. As shown in Fig. 6j, RIPK3 deficiency reduced infiltration of $CXCR3^+$ cells. Furthermore, dual-labeling with CD8 antibody showed that the infiltration of $CD8^+CXCR3^+$ cells was reduced in the lung tissue of infected $Ripk3^{-/-}$ mice (Fig. 6j). These results together indicate the important role of ZBP1-RIPK3 pathway in SARS-CoV-2-induced immune cell infiltration and lung damage in vivo.

DISCUSSION

In this study, we showed that SARS-CoV-2 infection results in Z-RNA formation which triggers ZBP1-RIPK3-MLKL necroptosis pathway and leads to inflammatory cytokine secretion (Supplementary information, Fig. S10). Mechanistic investigation indicated that Z-RNA binding with Zα2 domain or ZBP1 association with RIPK3 through the RHIM domain are both important for ZBP1 signaling. Depletion of ZBP1 or RIPK3, or treatment with RIPK3 kinase inhibitor prevented MLKL phosphorylation, confirming their roles in SARS-CoV-2-induced necroptosis activation. While the kinase activity of RIPK3 is important for necroptosis activation and inflammatory cytokine secretion, depleting RIPK3, which also impaired RIPK3's scaffolding functionality, reduced the production of both inflammatory cytokines and chemokines. In SARS-CoV-2-infected mouse model, depleting ZBP1 or RIPK3 reduced infiltration of multiple immune cell types and alleviated lung damage. Particularly, infiltration of neutrophils, macrophages and T cells was reduced. Infiltration of T cells and macrophages has been observed in critical COVID-19 patients[31] and is proposed to lead to severe disease development.[32] A recent study of SARS-CoV-2 infection in rhesus macaque model reported the correlation between $CXCR3^+$ cell infiltration and virus-induced lung damage and proposed the potential application of quantifying $CXCR3^+$ cells in predicting COVID-19 severity.[30] The result that ZBP1 or RIPK3 deficiency strongly reduced $CXCR3^+$ and $CD8^+CXCR3^+$ cell infiltration into the lung of SARS-CoV-2-infected mice further supports the critical role of ZBP1-RIPK3 axis in virus-induced lung pathogenesis.

T cells and macrophages are recruited through chemokines CXCL10 and CCL2,[33,34] respectively. Depleting RIPK3 significantly reduced both CXCL10 and CCL2 production in infected mouse model. In contrast, blocking necroptosis alone, either through drug treatment or through MLKL depletion, did not affect CXCL10 and CCL2 chemokine production or T cell and macrophage infiltration in vivo. These results suggest that the scaffolding function of RIPK3 is important for inflammatory signaling during SARS-CoV-2 infection. The RIPK1's kinase activity-independent scaffold function in regulating pro-survival (BCL-2 and XIAP) and inflammatory gene expression has been well described.[35,36] During the revision of this work, a study reported that scaffolding functionality of RIPK3 is important in ZBP1-induced inflammatory signaling[37] and the relevance of RIPK3 kinase independent role in inflammatory signaling awaits investigation in the context of virus infection. Here, we demonstrated the importance of RIPK3 scaffolding functionality in mediating inflammation in the context of SARS-CoV-2 infection in vitro and in animal model. The underlying mechanisms of RIPK3's scaffolding functionality in regulating inflammatory signaling during virus infection warrant further investigation.

Pathogen infection can trigger autocrine TNF production which can leads to RIPK1-RIPK3-MLKL-dependent necroptosis.[38–41] SARS-CoV-2 infection triggers TNF-α production and it is therefore possible that a parallel RIPK1-RIPK3-MLKL-dependent necroptosis pathway also contributes to the virus-induced inflammation. This notion is consistent with a recent study reporting that SARS-CoV-2 infection triggers RIPK1 activation which contributes to viral inflammation.[42] Nevertheless, RIPK3 is the critical adaptor mediating both necroptosis pathways and targeting RIPK3 is an attractive strategy to develop anti-inflammation drugs in the context of virus infection. Several RIPK3 kinase inhibitors have been developed for RIPK-driven inflammatory diseases.[35] Results from this study suggest that the anti-inflammation drug development targeting the scaffolding functionality of RIPK3 should also be considered, which might achieve an improved efficacy.

ZBP1 is an emerging innate sensor that recognizes Z-RNA as its natural ligand and activates the ZBP1-RIPK3-MLKL necroptosis pathway during virus infection.[17] Z-RNA was not thought to readily occur in natural settings because they are energetically less-favorable conformations of dsRNA.[18] Whether and how viruses form viral Z-RNA has become an important research topic in recent years.[18] In the case of VACV, binding of viral E3 protein dsRBD domain with viral RNA promotes Z-RNA formation.[14] While the mechanism of IAV Z-RNA formation is currently enigmatic, the defective viral genome is proposed to be the primary source of Z-RNA that triggers ZBP1 activation, potentially due to its production in great excess during IAV replication.[17] How the SARS-CoV-2 genome forms Z-RNA awaits further investigation. It has been shown that SARS-CoV-2 forms dsRNA during viral genome replication.[19] Whether association with viral protein is needed for SARS-CoV-2 dsRNA genome to produce Z-RNA, as is the case for VACV, is currently unknown.

Due to the technical difficulties of detecting Z-RNA, characterization of virus-induced Z-RNAs has been achieved only very recently.[14,17] Viral Z-RNA has been demonstrated for both DNA virus (such as VACV) and negative-stranded RNA virus (such as IAV). We now show here that SARS-CoV-2, which is a positive-stranded RNA virus, also forms Z-RNA to trigger the ZBP1-RIPK3-MLKL necroptosis pathway. These results indicate that Z-RNA might be a common RNA virus-derived PAMP during infection that triggers innate immune responses. Whether other RNA viruses that trigger necroptosis also produce Z-RNA to activate the ZBP1-RIPK3-MLKL pathway would be an interesting question for further investigation.

MATERIALS AND METHODS

Cell lines

Calu-3 cells were obtained from American Type Culture Collection (ATCC) and maintained in minimum Eagle's medium (MEM; Gibco) supplemented with 1% MEM Non-essential Amino Acids (Gibco), 1% Sodium Pyruvate

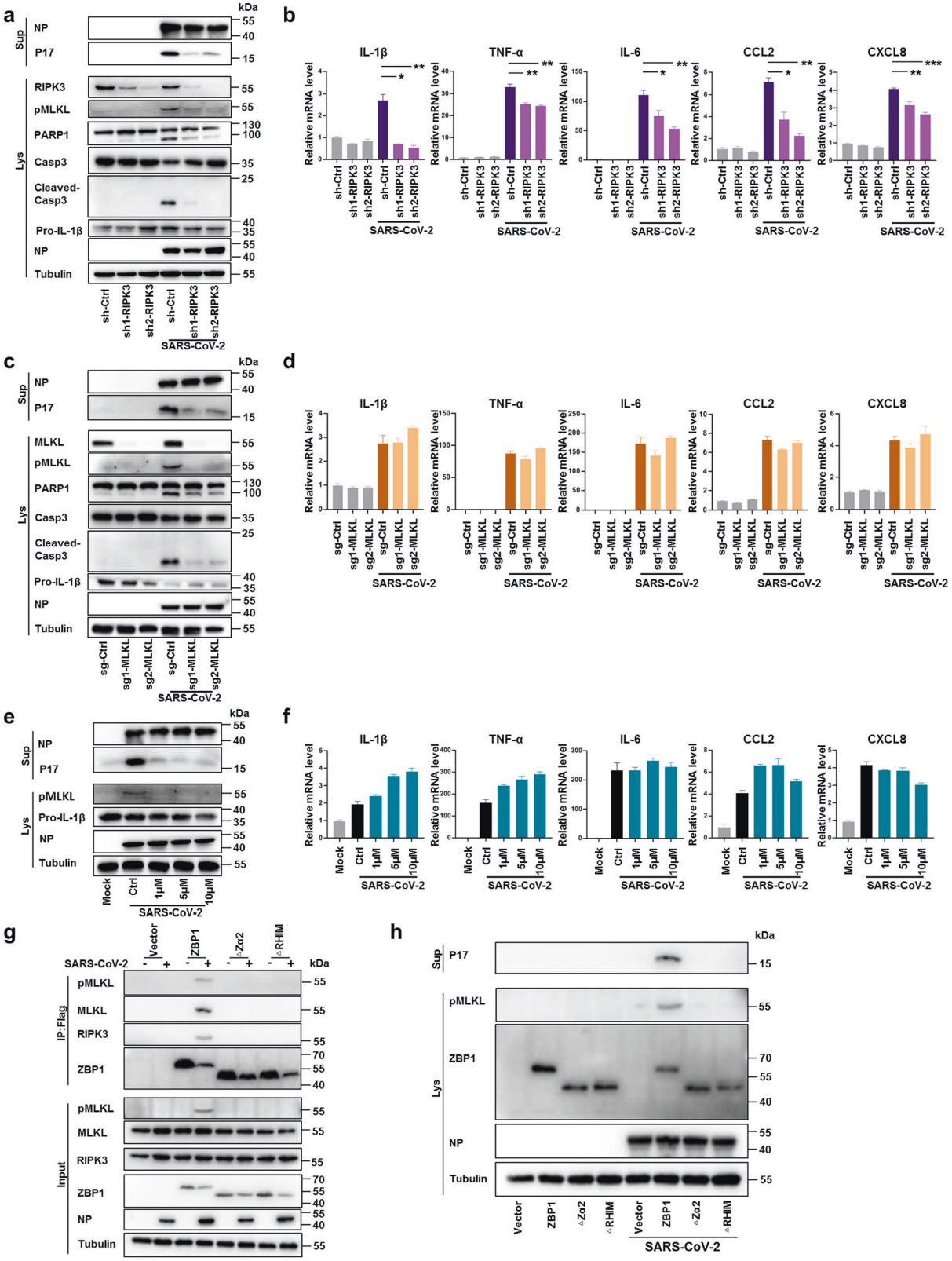

(100 mM, Gibco), 10% Fetal Bovine Serum (FBS; Gibco) and 1% antibiotics (Gibco). Vero E6 cells were obtained from ATCC and cultured in Dulbecco's modified Eagle's medium (DMEM; Gibco) supplemented with 10% FBS and 1% antibiotics. Cells were cultured in a humidified atmosphere of 5% CO_2 at 37 °C.

Viruses

The SARS-CoV-2 original strain (IVCAS 6.7512),[43] Alpha (B1.1.7), Beta (B1.351), Delta (B1.617.2), Omicron (B1.1.529) and the mouse-adapted virus (WBP-1)[29] were obtained from National Virus Resource Center and propagated in Vero E6 cells. Viral titer ($TCID_{50}$) was determined on Vero

Fig. 4 RIPK3 regulates SARS-CoV-2-induced necroptosis and inflammatory signaling. a, **b** Calu-3 cells stably expressing non-targeting shRNA (scramble) or shRNAs against RIPK3 were infected with SARS-CoV-2 at MOI of 0.1. Cells and supernatants were harvested at 48 hpi. **a** NP and P17 levels in supernatants and expression levels of RIPK3, pMLKL, PARP1, Casp3, cleaved-Casp3, Pro-IL-1β or NP in cell lysates were determined by western blot assay. **b** Relative mRNA level of indicated cytokine and chemokine genes was detected by qRT-PCR. **c**, **d** Calu-3 cells stably expressing non-targeting sgRNA (scramble) or sgRNAs against MLKL were infected with SARS-CoV-2 (MOI = 0.1). Cells and supernatants were harvested at 48 hpi. **c** NP and P17 levels in supernatants and expression levels of MLKL, pMLKL, PARP1, Casp3, cleaved-Casp3, Pro-IL-1β or NP in cell lysates were determined by western blot assay. **d** Relative mRNA level of indicated cytokine and chemokine genes was detected by qRT-PCR. **e**, **f** Calu-3 cells were pre-treated with GSK872 at concentration of 1, 5 or 10 μM followed by infection with SARS-CoV-2 (MOI = 0.1) for 48 h. **e** NP and P17 level in the supernatants, pMLKL, pro-IL-1β or NP in cell lysates were measured by western blot assay. **f** Relative mRNA level of indicated cytokine and chemokine genes was determined by qRT-PCR. **g**, **h** ZBP1 knockout Calu-3 cells reconstituted with FLAG-tagged full-length ZBP1or truncation mutants deleted of Zα2 domain (ZBP1-ΔZα2) or RHIM domain (ZBP1-ΔRHIM) were infected with SARS-CoV-2 (MOI = 0.1) or mock treated. **g** Cell lysates were harvested at 72 hpi and immunoprecipitated with anti-Flag magnetic beads, and detected by western blot assay. **h** Cell lysates and supernatant were harvested at 48 hpi. IL-1β P17 levels in the supernatants and the expression level of pMLKL, ZBP1or NP in the cell lysates were determined by western blot analysis. Data shown are means ± SEM. Statistical significance was analyzed by Student's *t*-test. $^{*}P < 0.05$; $^{**}P < 0.01$; $^{***}P < 0.001$.

E6 cells as described previously.[23] The SARS-CoV-2 infection experiments were performed in biosafety level-3 (BSL-3) laboratory.

Antibodies and reagents

Rabbit monoclonal anti-MLKL (#14993), anti-pMLKL (S358, used in western blot, #91689), anti-RIPK3 (#13526), anti-pRIPK3 (#91702) and rabbit polyclonal anti-ZBP1 (#60968), anti-cleaved Caspase-3 (#9661) were acquired from Cell Signaling Technology (Beverly, MA, USA). Rabbit polyclonal anti-IL-1β (A16288) was purchased from Abclonal (Wuhan, China). Rabbit polyclonal anti-CD45 (20103-1-AP), anti-α-tubulin (11224-1-AP) and mouse IgG (B900620) were obtained from Proteintech (Chicago, IL, USA). Rabbit monoclonal anti-pMLKL (S358, used in IFA, ab187091), anti-CD3 (ab237721), anti-CD4 (ab183685), anti-CD8 (ab217344) and anti-MPO (ab208670) were acquired from Abcam (Cambridge, UK). Rabbit monoclonal anti-pMLKL (S345, used in IHC, MA5-32752) was obtained from Thermo Fisher (Waltham, MA, USA). Rabbit polyclonal anti-CD68 (BA3638) was acquired from Boster Biological Technology (Wuhan, China). Mouse monoclonal antibody anti-Z-DNA (Ab00783-3.0) was purchased from Absolute antibody (Oxford, UK). Rabbit-anti-SARS-CoV-2-NP antibody and mouse-anti-SARS-CoV-2-NP (SR24) antibody were made in house. GSK872 (HY-101872) was acquired from MedChemExpress (New Jersey, USA). 4,6-diamidino-2-phenylindole (DAPI, C1002) was obtained from Beyotime (Shanghai, China).

RNA isolation, cDNA library preparation and sequencing

Calu-3 cells were infected with SARS-CoV-2 at an MOI of 0.1 or mock treated. At 12, 24, 36, 48 hpi, cells were harvested and total RNA was extracted with FastPure Cell/Tissue Total RNA Isolation Kit (Vazyme, China) according to the manufacturer's instructions. The quality of total RNA was assessed with NanoPhotometer spectrophotometer (Implen, Germany) and Agilent 2100 BioAnalyzer (Agilent Technologies, Santa Clara, CA, USA). Total RNA samples meeting the quality requirements were used to generate RNA-seq libraries, and then sequenced by CapitalBio Technology (Beijing, China). The final libraries were quantified using Agilent 2100 Bioanalyzer and subjected to paired-end sequencing using Illumina Novaseq 6000 (Illumina, San Diego, CA, USA).

Data analysis of RNA-seq

The human genome sequence version hg19 was used as reference to analyze the RNA-seq data. The quality of sequencing was assessed with FastQC (v0.11.8). The clean reads were obtained by using SOAPnuke (v1.3.0) to filter the low quality data, and aligned to the reference genome by STAR (v2.7.0) with default parameters. The processed reads from each sample were aligned with STAR against the reference sequence. The gene expression analyses were performed with Htseq (v0.11.2). DESeq (v1.28.0) was used to analyze the DEGs between samples. The *P*-value was corrected by FDR method to obtain the q value, which was used to conduct significance analysis. Parameters for classifying significant DEGs are 2-fold differences ($|\log_2 FC| \geq 1$, FC, the fold change of expressions) in the transcript abundance and $q < 0.05$.

Knockout by CRISPR-Cas9 technology

Knockout of ZBP1 or MLKL was done through lentiviral transduction of Calu-3 cells. Briefly, Calu-3 cells were transduced with lentiviruses expressing Cas9 and specific small-guide RNAs (sgRNAs) for 24 h and selected by puromycin (8 μg/mL). Due to the growth characteristic of Calu-3 cells, polyclonal pools of transduced cells were used for subsequent experiments. Sequences of sgRNAs targeting specific genes used in this study are shown in Supplementary information, Table S1.

Knockdown of RIPK3

RIPK3 was knocked down through lentiviral transduction of Calu-3 cells as described above. Sequences of targeting shRNA used in this study are shown in Supplementary information, Table S2.

qRT-PCR

qRT-PCR was performed with a two-step procedure using the HiScript III 1st Strand cDNA Synthesis Kit (Vazyme, China) and ChamQ Universal SYBR quantitative PCR Master Mix (Vazyme, China). Viral load was determined by quantification of copies of SARS-CoV-2 S gene in samples, and a known copy number plasmid containing S gene was used as a standard for copy number quantification. Primer sequences are shown in Supplementary information, Table S3.

Western blot analysis

Cells infected and treated as indicated were collected and lysed with the cell lysis buffer (Beyotime, China). Cell lysates were subjected to 12% SDS-polyacrylamide gel electrophoresis (PAGE) and then transferred to polyvinylidene difluoride (PVDF) membranes (Millipore). After blocking, proteins were incubated with the indicated primary antibodies and then corresponding horseradish peroxidase-conjugated secondary antibodies. Protein bands were detected by Chemiluminescence Analyzer (Chemiscope600pro) using an enhanced chemiluminescence (ECL) kit (Millipore).

Annexin/PI staining

Calu-3 cells were infected with SARS-CoV-2 (MOI = 0.1). At the indicated hours post infection, cells were stained with Annexin and PI by Annexin V-FITC Apoptosis Detection Kit (Beyotime, China), following the instructions.

Mature IL-1β detection

The extraction of protein in the collected supernatant was conducted as described previously.[23] Briefly, equal volume of methanol and a quarter volume of chloroform were used to precipitate the proteins in cell culture supernatant. The precipitant was dissolved and subjected to western blot analyses using antibodies against IL-1β (ABclonal, China).

IFA

Calu-3 cells were infected with SARS-CoV-2 original strain (MOI = 0.1) or mock treated. At 48 hpi, cells were fixed, permeabilized and blocked. For the detection of the localization of pMLKL, the cells were incubated with rabbit anti-pMLKL (S358, Abcam) and mouse anti-NP (SR24) as primary antibodies. For the detection of Z-RNA generation, infected cells were fixed and permeablized, followed by RNase A (2 mg/ml) or DNase I (25 U/mL) treatment for 2 h at 37 °C or left untreated, blocked and incubated with rabbit anti-NP and mouse anti-Z-DNA (Z22 clone, Absolute antibody). For the co-staining of ZBP1 and Z-RNA, infected cells were fixed and incubated with rabbit anti-ZBP1 and mouse anti-Z-DNA. For the staining of Z-RNA in VOC-infected cells, Calu-3 cells were infected with SARS-CoV-2 Alpha, Beta,

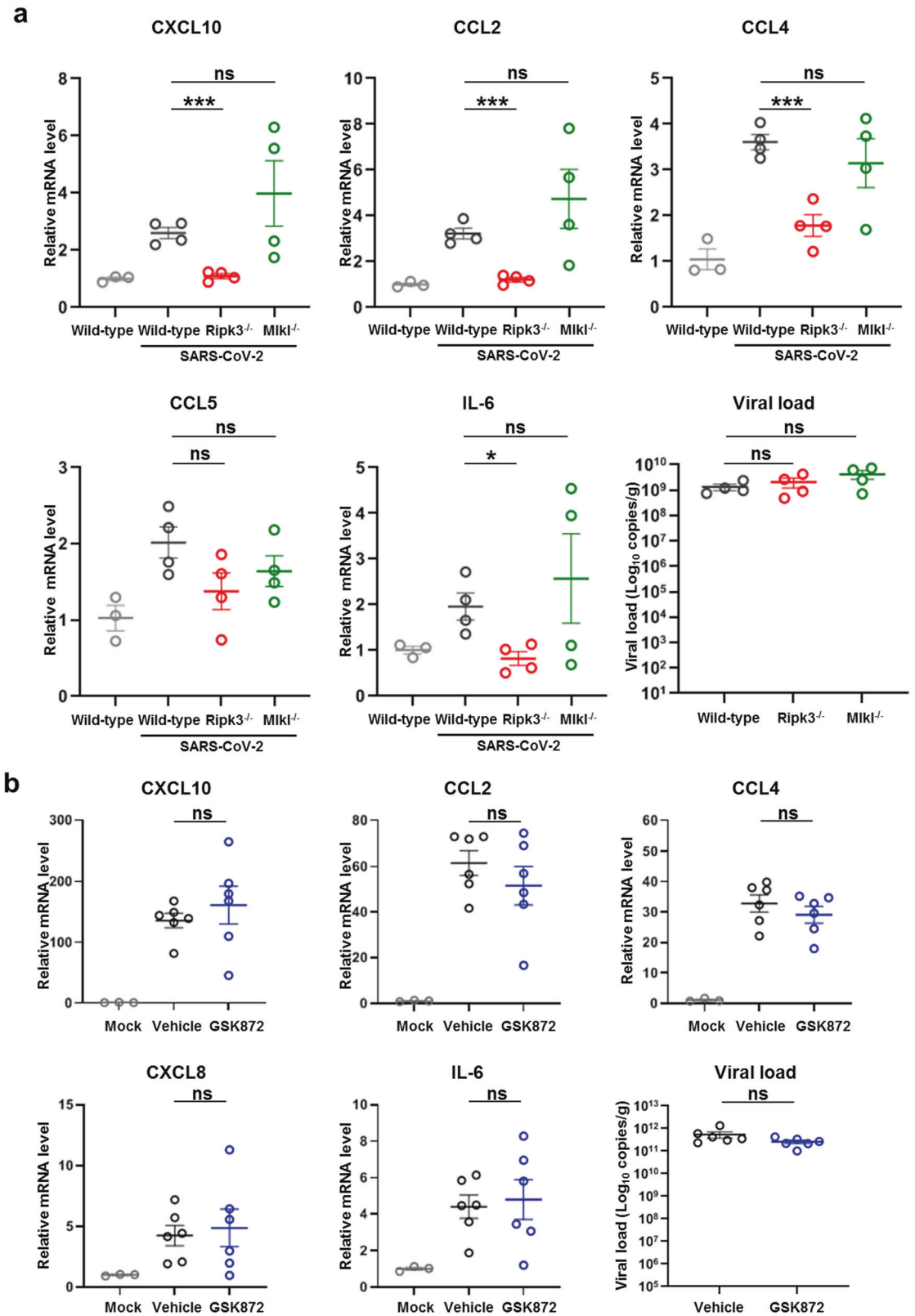

Fig. 5 The scaffolding function of RIPK3 is critical for SARS-CoV-2-triggered inflammatory chemokine production in the lung. a Ripk3$^{-/-}$ Mlkl$^{-/-}$ or wild-type C57BL/6 mice ($n = 4$) were intranasally transduced with Ad5-hACE2 (2.5×10^8 PFU) and infected with SARS-CoV-2 (1×10^5 $TCID_{50}$) at 5 days post transduction. Ad5-hACE2 transduced but uninfected wild-type C57BL/6 mice ($n = 3$) were used as the control. Lung samples were harvested at 2 dpi. Relative mRNA level of indicated genes was analyzed with qRT-PCR and normalized to samples from transduced but uninfected wild-type mice. **b** The effect of GSK872 on SARS-CoV-2-induced upregulation of cytokines and chemokines in the lung. BALB/c mice were intranasally infected with the mouse-adapted virus (WBP-1, 1×10^4 $TCID_{50}$) and treated with vehicle ($n = 6$) or GSK872 (10 mg/kg/d) ($n = 6$) by intraperitoneal injection. Mice were euthanized at 5 dpi and lung samples were harvested for qRT-PCR determination. Data shown are means ± SEM. Statistical significance was analyzed by Student's *t*-test. $^*P < 0.05$; $^{***}P < 0.001$; ns, no significance.

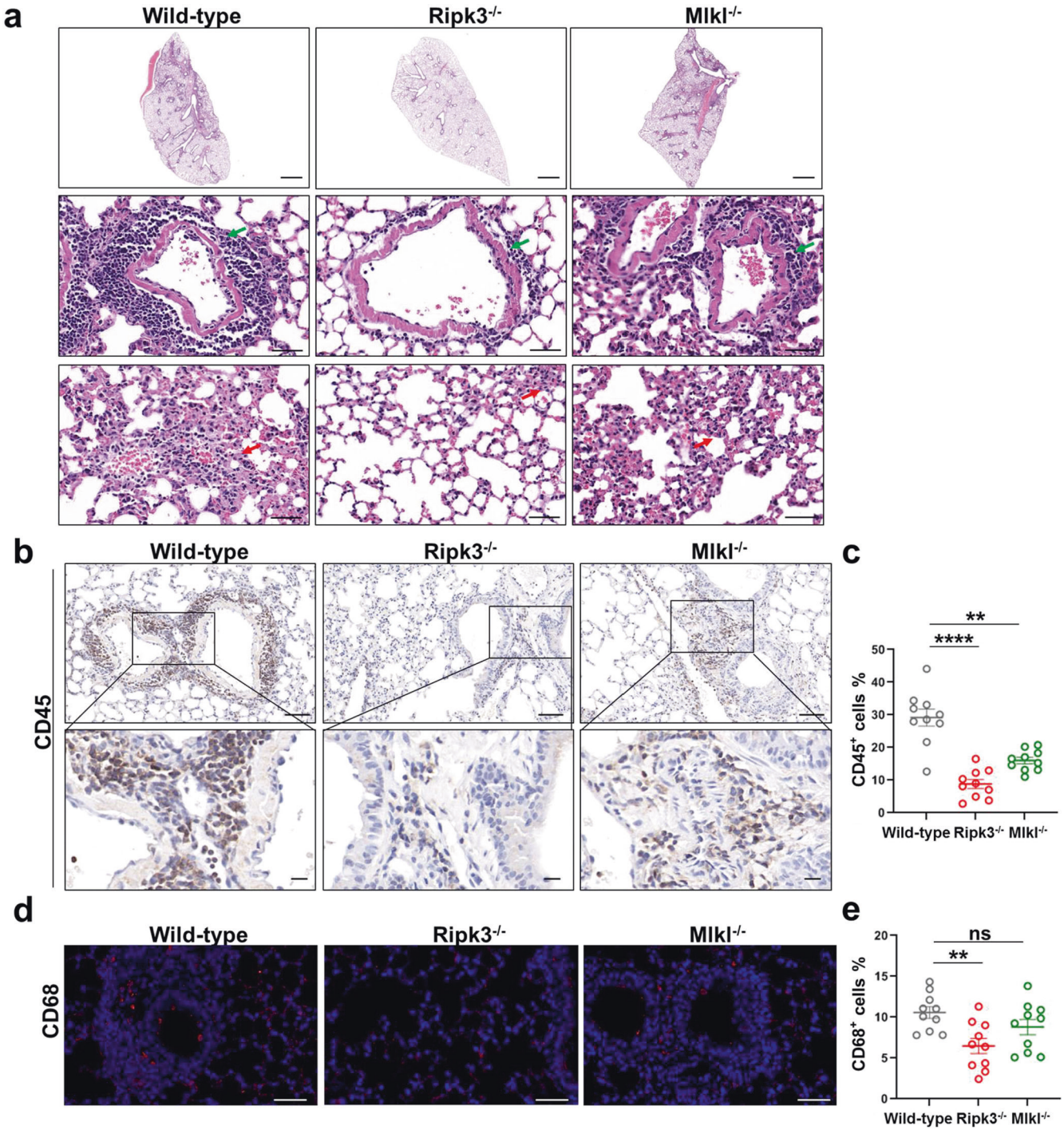

Fig. 6 RIPK3 contributes to SARS-CoV-2-induced lung damage and immune cell infiltration into the lung. a–e Ad5-hACE2 (2.5×10^8 PFU) transduced Ripk3$^{-/-}$, Mlkl$^{-/-}$ or wild-type C57BL/6 mice were infected with SARS-CoV-2 (1×10^5 $TCID_{50}$). Lung samples were harvested at 2 dpi. **a** The histopathological changes were evaluated by H&E staining. Inflammatory cell infiltration (green arrow) and alveolar septa expansion (red arrow) were indicated. Scale bars, 1000 μm in the original image and 50 μm in the enlarged image. **b–j** Immunostaining of CD45 (**b**), CD68 (**d**), CD3 (**f**) and MPO (**h**) representing the infiltration of leukocytes, macrophages, T cells and neutrophils respectively. **b**, **f** Scale bars, 50 μm and 10 μm in the enlarged image. **d**, **h** Scale bars, 50 μm. **c**, **e**, **g**, **i** Quantitative analysis of positive cells performed with ImageJ for **b**, **d**, **f**, **h**, respectively. Data shown are means ± SEM. Statistical significance was analyzed by Student's *t*-test. *$P < 0.05$; **$P < 0.01$; ***$P < 0.001$; **** $P < 0.0001$; ns, no significance. **j** Co-staining of CD8 (red) and CXCR3 (green) representing the recruitment of $CD8^+CXCR3^+$ T cells in the lung section of SARS-CoV-2-infected wild-type and Ripk3$^{-/-}$ mice. Scale bars, 10 μm.

Delta or Omicron strains (MOI = 0.1) or mock treated for 48 h, and stained with antibodies against NP and Z-DNA. Then cells were incubated with Fluor 488 goat anti-rabbit IgG and Fluor 561 goat anti-mouse IgG for 1 h. Cells were then washed and incubated with DAPI (Beyotime, China), and analyzed using confocal microscope (Andor Dragonfly 202).

RNA immunoprecipitation

Calu-3 cells were infected with SARS-CoV-2 original strain (MOI = 0.1), and were lysed with lysis buffer (Beyotime, China) supplemented with protease and RNase inhibitor for RNA immunoprecipitation (RIP) at 48 hpi. Cell lysate were incubated with Z-NA antibody (Z22 clone, Absolute antibody) or

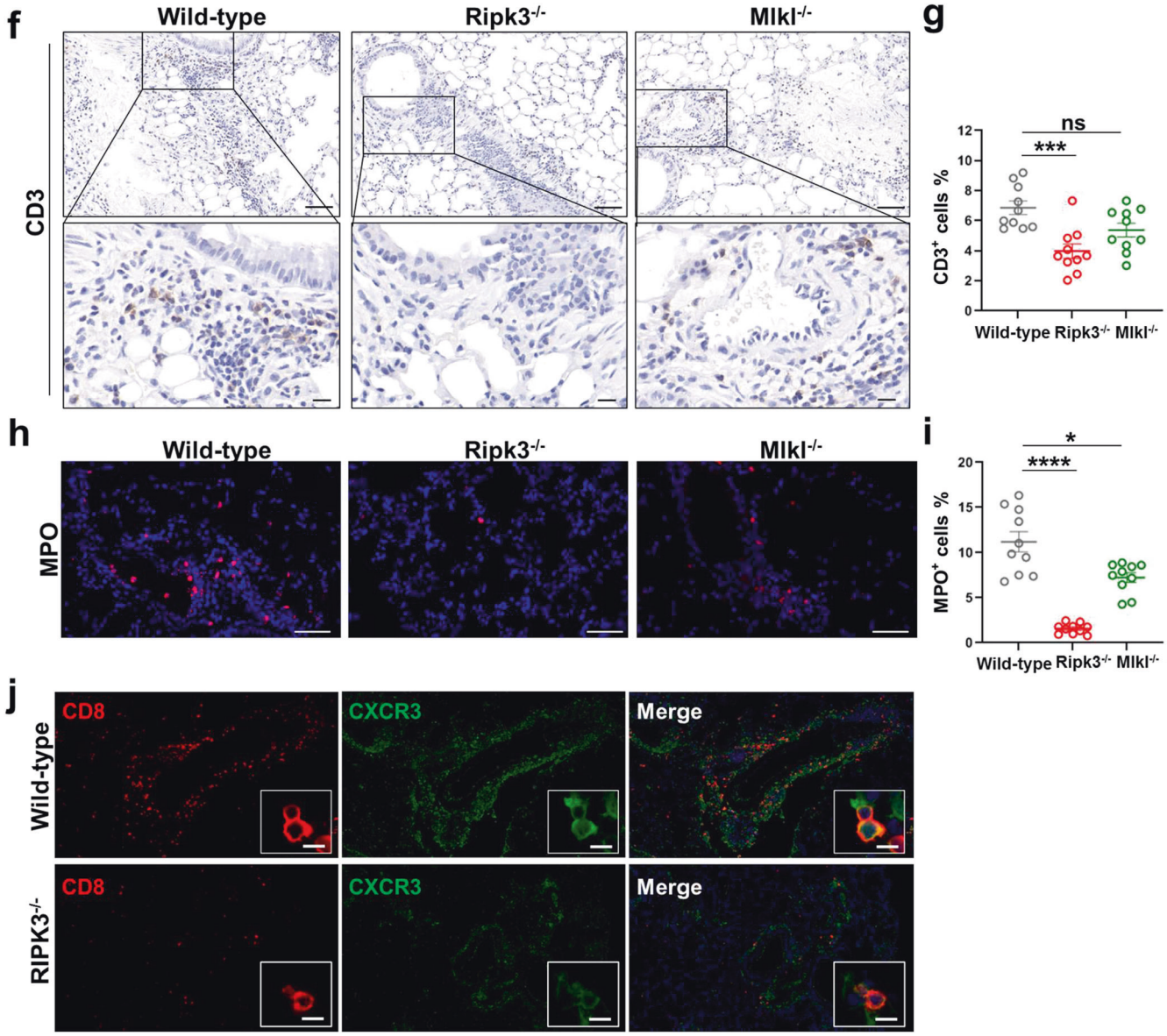

isotype mouse IgG at 4 °C overnight, followed by incubation with Pierce Classic Magnetic beads (Thermo Fisher Scientific) for 1 h at room temperature. After washing, beads were incubated with proteinase K and DNAse I and RNA were purified with RNA extraction kit (TAKARA) and subjected to qRT-PCR analysis.

Flag immunoprecipitation

ZBP1-KO Calu-3 cells reconstituted with FLAG-tagged full-length ZBP1 or truncation mutants were infected with SARS-CoV-2 original strain (MOI = 0.1) or mock treated and lysed in lysis buffer (Beyotime, China) supplemented with protease and phosphatase inhibitor (Thermo Fisher Scientific) at 72 hpi. Cell lysates were incubated with anti-Flag magnetic beads (Beyotime, China) at 4 °C overnight. After washing, beads were eluted and subjected to western blot analysis as described before.

Animal study

An adenoviral transduction-based strategy was used in Zbp1$^{-/-}$, Ripk3$^{-/-}$ or Mlkl$^{-/-}$ mouse transduction experiment.[26] Briefly, KO mice and littermate control mice of the C57BL/6 background were intranasally transduced with Ad5-hACE2 (2.5×10^8 PFU), and intranasally infected with SARS-CoV-2 (1×10^5 $TCID_{50}$) 5 days after transduction. Mice were euthanized at 2 dpi and lung samples were harvested for qRT-PCR determination, histology and immunohistochemistry. As for Zbp1$^{-/-}$ mouse experiment, both Zbp1$^{-/-}$ and wild-type C57BL/6 mice were divided into three groups: non-transduced and non-infected group ($n = 3$), transduced but non-infected group ($n = 3$), transduced and infected group ($n = 6$). As for Ripk3$^{-/-}$ or Mlkl$^{-/-}$ experiment, mice were divided into four groups: transduced but non-infected wild-type mice ($n = 3$), transduced and infected wild-type ($n = 4$), Ripk3$^{-/-}$ ($n = 4$) or Mlkl$^{-/-}$ mice ($n = 4$).

For the assessment of GSK872 treatment base on mouse-adapted SARS-CoV-2 model, 6–8-week-old female BALB/c mice were divided into three groups: SARS-CoV-2 infection treated with vehicle group ($n = 6$), SARS-CoV-2 infection treated with GSK872 group ($n = 6$), and DMEM treatment group ($n = 3$). Mice were intranasally infected with mouse-adapted SARS-CoV-2 (WBP-1, 1×10^4 $TCID_{50}$) or the same volume of DMEM. GSK872 was given by intraperitoneal injection with the dose of 10 mg/kg/d after inoculation. The drug was administered on a daily basis and mice were euthanized at 5 dpi. Lung samples were harvested for qRT-PCR determination and immunohistochemistry.

For the assessment of GSK872 treatment based on adenoviral transduction model, 8–10-week-old male C57BL/6 mice were divided into three groups: SARS-CoV-2 infection treated with vehicle group ($n = 4$), SARS-CoV-2 infection treated with GSK872 group ($n = 4$), and DMEM treatment group ($n = 3$). Mice were intranasally transduced with Ad5-hACE2 (2.5×10^8 PFU), and intranasally infected with SARS-CoV-2 (1×10^5 $TCID_{50}$) 5 days after transduction. GSK872 was given by intraperitoneal injection with the dose of 10 mg/kg/d after inoculation.

The drug was administered on a daily basis and mice were euthanized at 2 dpi. Lung samples were harvested for qRT-PCR determination and immunohistochemistry.

Animal experiments were approved by Wuhan Institute of Virology animal welfare committee.

Histology and immunohistochemistry

Lung samples obtained from infected and mock-infected mice were fixed with 4% paraformaldehyde, embedded in paraffin and cut into sections of 4 μm, and further used for histology or immunohistochemistry (IHC). For histology, lung sections were stained with Gill's haematoxylin and eosin-Y. For IHC, the indicated antibodies were used as primary antibodies, then sections were incubated with secondary antibody (Rabbit/Mouse Envision, Dako, Denmark), and visualized with a detection kit (DAB, Dako, Denmark). Immunostaining was performed using indicated primary antibodies and followed by incubation with Fluor 561 secondary antibody and DAPI.

REFERENCES

1. Hu, B., Guo, H., Zhou, P. & Shi, Z. L. Characteristics of SARS-CoV-2 and COVID-19. *Nat. Rev. Microbiol.* **19**, 141–154 (2021).
2. Wiersinga, W. J., Rhodes, A., Cheng, A. C., Peacock, S. J. & Prescott, H. C. Pathophysiology, transmission, diagnosis, and treatment of Coronavirus disease 2019 (COVID-19): a review. *JAMA* **324**, 782–793 (2020).
3. Li, H. et al. SARS-CoV-2 and viral sepsis: observations and hypotheses. *Lancet* **395**, 1517–1520 (2020).
4. Tay, M. Z., Poh, C. M., Renia, L., MacAry, P. A. & Ng, L. F. P. The trinity of COVID-19: immunity, inflammation and intervention. *Nat. Rev. Immunol.* **20**, 363–374 (2020).
5. Mehta, P. et al. COVID-19: consider cytokine storm syndromes and immunosuppression. *Lancet* **395**, 1033–1034 (2020).
6. Angus, D. C. et al. Effect of hydrocortisone on mortality and organ support in patients with severe COVID-19: the REMAP-CAP COVID-19 corticosteroid domain randomized clinical trial. *JAMA* **324**, 1317–1329 (2020).
7. Dequin, P. F. et al. Effect of hydrocortisone on 21-day mortality or respiratory support among critically ill patients with COVID-19: a randomized clinical trial. *JAMA* **324**, 1298–1306 (2020).
8. Sterne, J. A. C. et al. Association between administration of systemic corticosteroids and mortality among critically ill patients with COVID-19: a meta-analysis. *JAMA* **324**, 1330–1341 (2020).
9. Horby, P. et al. Dexamethasone in hospitalized patients with Covid-19. *N. Engl. J. Med.* **384**, 693–704 (2021).
10. Tomazini, B. M. et al. Effect of dexamethasone on days alive and ventilator-free in patients with moderate or severe acute respiratory distress syndrome and COVID-19: the CoDEX randomized clinical trial. *JAMA* **324**, 1307–1316 (2020).
11. Nailwal, H. & Chan, F. K. Necroptosis in anti-viral inflammation. *Cell Death Differ.* **26**, 4–13 (2019).
12. Verdonck, S., Nemegeer, J., Vandenabeele, P. & Maelfait, J. Viral manipulation of host cell necroptosis and pyroptosis. *Trends Microbiol.* **6**, 593–605 (2021).
13. Chen, D. et al. RIP3-dependent necroptosis contributes to the pathogenesis of chronic obstructive pulmonary disease. *JCI Insight* **6**, e144689 (2021).
14. Koehler, H. et al. Vaccinia virus E3 prevents sensing of Z-RNA to block ZBP1-dependent necroptosis. *Cell Host Microbe* **29**, 1266–1276.e5 (2021).
15. Moriwaki, K. et al. The necroptosis adaptor RIPK3 promotes injury-induced cytokine expression and tissue repair. *Immunity* **41**, 567–578 (2014).
16. Zheng, M. & Kanneganti, T. D. The regulation of the ZBP1-NLRP3 inflammasome and its implications in pyroptosis, apoptosis, and necroptosis (PANoptosis). *Immunol. Rev.* **297**, 26–38 (2020).
17. Zhang, T. et al. Influenza virus Z-RNAs induce ZBP1-mediated necroptosis. *Cell* **180**, 1115–1129.e13 (2020).
18. Balachandran, S. & Mocarski, E. S. Viral Z-RNA triggers ZBP1-dependent cell death. *Curr. Opin. Virol.* **51**, 134–140 (2021).
19. Li, Y. et al. SARS-CoV-2 induces double-stranded RNA-mediated innate immune responses in respiratory epithelial-derived cells and cardiomyocytes. *Proc. Natl. Acad. Sci. USA* **118**, e2022643118 (2021).
20. Lin, J. W. et al. Genomic monitoring of SARS-CoV-2 uncovers an Nsp1 deletion variant that modulates type I interferon response. *Cell Host Microbe* **29**, 489–502.e8 (2021).
21. Mahoney, M. et al. A novel class of TMPRSS2 inhibitors potently block SARS-CoV-2 and MERS-CoV viral entry and protect human epithelial lung cells. *Proc. Natl. Acad. Sci. USA* **118**, e2108728118 (2021).
22. Christgen, S. et al. Identification of the PANoptosome: a molecular platform triggering pyroptosis, apoptosis, and necroptosis (PANoptosis). *Front. Cell. Infect. Microbiol.* **10**, 237 (2020).
23. Li, S. et al. SARS-CoV-2 triggers inflammatory responses and cell death through caspase-8 activation. *Signal Transduct. Target. Ther.* **5**, 235 (2020).
24. Takaoka, A. et al. DAI (DLM-1/ZBP1) is a cytosolic DNA sensor and an activator of innate immune response. *Nature* **448**, 501–505 (2007).
25. Upton, J. W., Kaiser, W. J. & Mocarski, E. S. DAI/ZBP1/DLM-1 complexes with RIP3 to mediate virus-induced programmed necrosis that is targeted by murine cytomegalovirus vIRA. *Cell Host Microbe* **11**, 290–297 (2012).
26. Sun, J. et al. Generation of a broadly useful model for COVID-19 pathogenesis, vaccination, and treatment. *Cell* **182**, 734–743.e5 (2020).
27. Jiao, H. et al. Z-nucleic-acid sensing triggers ZBP1-dependent necroptosis and inflammation. *Nature* **580**, 391–395 (2020).
28. Rebsamen, M. et al. DAI/ZBP1 recruits RIP1 and RIP3 through RIP homotypic interaction motifs to activate NF-kappaB. *EMBO Rep.* **10**, 916–922 (2009).
29. Huang, K. et al. Q493K and Q498H substitutions in spike promote adaptation of SARS-CoV-2 in mice. *EBioMedicine* **67**, 103381 (2021).
30. Zheng, H. Y. et al. Pro-inflammatory microenvironment and systemic accumulation of CXCR3+ cell exacerbate lung pathology of old rhesus macaques infected with SARS-CoV-2. *Signal Transduct. Target. Ther.* **6**, 328 (2021).
31. Desai, N. et al. Temporal and spatial heterogeneity of host response to SARS-CoV-2 pulmonary infection. *Nat. Commun.* **11**, 6319 (2020).
32. Nienhold, R. et al. Two distinct immunopathological profiles in autopsy lungs of COVID-19. *Nat. Commun.* **11**, 5086 (2020).
33. Harris, T. H. et al. Generalized Levy walks and the role of chemokines in migration of effector CD8+ T cells. *Nature* **486**, 545–548 (2012).
34. Qian, B. Z. et al. CCL2 recruits inflammatory monocytes to facilitate breast-tumour metastasis. *Nature* **475**, 222–225 (2011).
35. Martens, S., Hofmans, S., Declercq, W., Augustyns, K. & Vandenabeele, P. Inhibitors targeting RIPK1/RIPK3: old and new drugs. *Trends Pharmacol. Sci.* **41**, 209–224 (2020).
36. Silke, J., Rickard, J. A. & Gerlic, M. The diverse role of RIP kinases in necroptosis and inflammation. *Nat. Immunol.* **16**, 689–697 (2015).
37. Peng, R. et al. Human ZBP1 induces cell death-independent inflammatory signaling via RIPK3 and RIPK1. *EMBO Rep.* e55839 (2022).
38. Cho, Y. S. et al. Phosphorylation-driven assembly of the RIP1-RIP3 complex regulates programmed necrosis and virus-induced inflammation. *Cell* **137**, 1112–1123 (2009).
39. Carpenter, E. A., Ruby, J. & Ramshaw, I. A. IFN-gamma, TNF, and IL-6 production by vaccinia virus immune spleen cells. An in vitro study. *J. Immunol.* **152**, 2652–2659 (1994).
40. Polykratis, A. et al. Cutting edge: RIPK1 Kinase inactive mice are viable and protected from TNF-induced necroptosis in vivo. *J. Immunol.* **193**, 1539–1543 (2014).
41. Liu, Z. et al. A class of viral inducer of degradation of the necroptosis adaptor RIPK3 regulates virus-induced inflammation. *Immunity* **54**, 247–258.e7 (2021).
42. Xu, G. et al. SARS-CoV-2 promotes RIPK1 activation to facilitate viral propagation. *Cell Res.* **31**, 1230–1243 (2021).
43. Zhou, P. et al. A pneumonia outbreak associated with a new coronavirus of probable bat origin. *Nature* **579**, 270–273 (2020).

ACKNOWLEDGEMENTS

This work was supported by the National Key R&D Program of China (2018YFA0507201, 2021YFC2300702, 2022YFC2303302), the Strategic Priority Research Program of the Chinese Academy of Sciences (XDB29010204), Creative Research Group Program of Natural Science Foundation of Hubei Province (2022CFA021), the National Natural Science Foundation of China (32070179), Self-supporting Program of Guangzhou Laboratory (SRPG22-001), the Hundred Talents Program of Chinese Academy of Sciences (to Ke Peng), and the Advanced Customer Cultivation Project of Wuhan National Biosafety Laboratory, Chinese Academy of Sciences (2022ACCP-MS10). We would like to thank Dr Ding Gao, Ms Anna Du and Ms Juan Min, from the Center for Instrumental Analysis and Metrology, Wuhan Institute of Virology, Chinese Academy of Science for technical assistance. We would like to acknowledge Ms Xuefang An, Mr He Zhao, Ms Li Li and Ms Youling Zhu from the Center for Experimental Animals, Wuhan Institute of Virology for help in animal experiments. We thank Tao Du, Jia Wu, Hao Tang and Jun Liu from the BSL-3 Laboratory, Wuhan Institute of Virology for their essential support.

AUTHOR CONTRIBUTIONS

K.P., P.Z. and B.L. conceived and supervised the study. K.P., P.Z., B.L., S.L., Y.Z. and Z.G. participated in the study design, analyzed the data, and wrote the manuscript. S.L., Y.Z., Z.G., M.D.Y., H.L., M.M.Y., C.Z. and Z.Z. performed the experiments. All authors read and approved the manuscript.

COMPETING INTERESTS

The authors declare no competing interests.

ADDITIONAL INFORMATION

Supplementary information The online version contains supplementary material available at https://doi.org/10.1038/s41422-022-00775-y.

Correspondence and requests for materials should be addressed to Ben Lu, Peng Zhou or Ke Peng.